
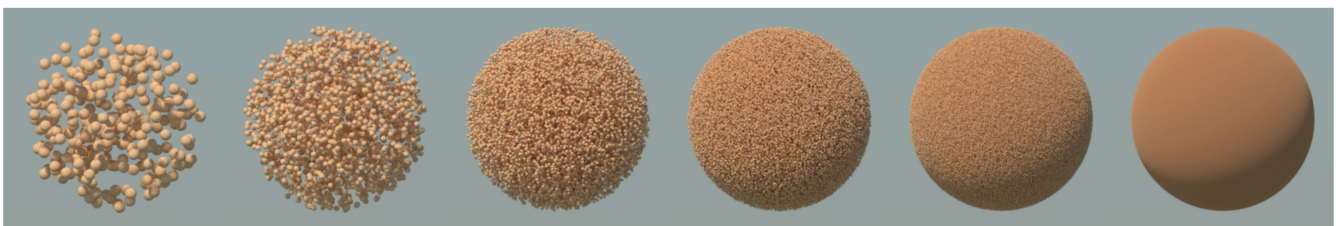


# An analytic BRDF for materials with spherical Lambertian scatterers

Eugene d'Eon 

NVIDIA

Autodesk



**Figure 1:** We derive a new analytic BRDF (right) for porous materials where scattering and absorption is well approximated by spherical Lambertian particles. Here we show a sequence of stochastic microgeometries consisting of independent random placement of opaque Lambertian spheres occupying 7% of the volume. As the scale of the microgeometry is varied inside the fixed spherical domain, the appearance approaches our BRDF where no spatial variability is resolved across pixels.

## Abstract

We present a new analytic BRDF for porous materials comprised of spherical Lambertian scatterers. The BRDF has a single parameter: the albedo of the Lambertian particles. The resulting appearance exhibits strong back scattering and saturation effects that height-field-based models such as Oren-Nayar cannot reproduce.

## CCS Concepts

• Computing methodologies → Reflectance modeling;

## 1. Introduction

The *bidirectional reflectance distribution function* (BRDF) is a fundamental building block in computer graphics and other fields. BRDF measurements have shown that real world materials exhibit a wide range of reflectance behaviours [MPBM03, DJ18]. While measured data can be used directly, it is bulky and difficult to edit. In contrast, parametric BRDFs are compact and permit artist control, but no one parametric BRDF spans the full breadth of real-world appearances. It is therefore important to define a small set of flexible analytic parametric BRDFs that cover a wide range of materials.

The most popular parametric BRDFs derive from Smith's [Smi67] geometrical and statistical treatment of random height fields [CT82, Bli82, vGSK98, Sta01, WMLT07, Hei14]. These models support a variety of surface statistics [RBMS17], anisotropy [Hei14], importance sampling [Hd14] and multiple scattering with specular, diffuse, or mixed microfacets [HD15, HHdD16,

MBT\*17]. These BRDFs have been highly successful and cover a wide range of materials, but the assumption of a height field is not always valid [Dhd16]: these BRDFs cannot model *porous/granular/volumetric/particulate* microgeometry, such as the synthetic example shown in Figure 1 or the surface profiles of materials such as carbon soot [SOPB08].

To simulate a wide range of diffusive behaviours that extend beyond the limitations of a diffuse heightfield, *volumetric* BRDFs can be derived by considering scalar radiative transfer in slabs under a plane-parallel assumption [vdH80, Yan97, KP03]. This models the microstructure as a randomly distributed array of absorbing and scattering particles in a volume. Multiple volumetric slabs can be interleaved between random height fields to form fully general layer stacks [Sta01] that can be stochastically evaluated in a “position-free” way [GHZ18] or numerically pretabulated using adding/doubling or related methods [Sta01, JdJM14, ZJ18, Bel18]. A great variety of parametric layered materials can be evaluated using these methods, but they can significantly exceed the complex-

ity, cost and memory requirements of simpler analytical BRDFs. More efficient layering is possible [WW07], but at the cost of losing reciprocity and accuracy. One exception is the half space with isotropic scattering, which has a known semi-analytic BRDF (Chandrasekhar's BRDF) [Cha60, KC17].

Chandrasekhar's BRDF is the unique exact volumetric BRDF that can be applied as efficiently and broadly as other analytic height-field BRDFs. It has inspired BRDFs for lunar regoliths [Hap81] and has been extended to support Fresnel reflection at the boundary [WNO98, Wil06]. A stochastic geometry that is consistent with Chandrasekhar's BRDF (under geometrical-optics) is a sparse suspension of mirror sphere particles in a purely absorbing matrix. In this paper we derive what is the Oren-Nayar [ON94] equivalent of this BRDF, by making the scatterers white Lambertian spheres. By the equivalence principle of classical radiative transfer [vdH80], this is equivalent to a void matrix with absorbing Lambertian spherical particles. The result is a new approximate analytic BRDF for dusty/porous materials (Figure 1) that offers a distinct appearance from Oren-Nayar's height field BRDF and from azimuthally-symmetric diffuse BRDFs such as Chandrasekhar's and Disney's diffuse BRDF [Bur12].

We begin by recalling the far-field phase function for a Lambertian sphere in section 2. We derive importance-sampling and adding-doubling integrals for this phase function and note that it is well approximated by a three-term Legendre expansion. This allows application of a known result for the exact BRDF of a three-term halfspace, which we use in section 3 to derive an accurate analytic approximation for the Lambert sphere BRDF. The result is more accurate than previous general approximations that assume azimuthally-symmetric multiple scattering [Hap81, Hap02]. In section 4 we compare the appearance of the new BRDF to previous analytic diffuse BRDFs and also compare the performance in layered material configurations using both position-free and doubling approaches.

## 2. Lambertian sphere phase function

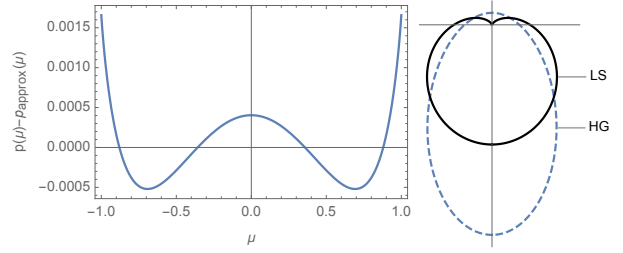
The far-field geometrical-optics phase function for a smooth, white Lambertian sphere (LS) is [Bli82]

$$p(\mu) = \frac{2(\sqrt{1-\mu^2} - \mu \cos^{-1}(\mu))}{3\pi^2} = \frac{2(\sin(\theta) - \theta \cos(\theta))}{3\pi^2} \quad (1)$$

where  $\mu = \cos\theta$ . This phase function was first derived by Lambert himself in 1760, complete with an accurate numerical table [Lam60, p.471]. The mean cosine of the LS phase function is  $g = -4/9 \approx -0.444444$  and, unlike many parametric models, it scatters no light directly forward,  $p(1) = 0$ . The overall behaviour of this phase function is sufficiently distinct from other popular parametric models such as Henyey-Greenstein (HG) [Bli82] to warrant a unique investigation (see Figure 2 [right] where we compare to HG with the same mean cosine).

For the Legendre expansion of the LS phase function

$$p(\mu) = \frac{1}{4\pi} \sum_{k=0}^{\infty} A_k P_k(\mu), \quad (2)$$



**Figure 2:** Left: A three-term Legendre expansion of the phase function of the Lambertian sphere (LS) particle is accurate to within 0.2%. Right: The LS phase function is significantly different from Henyey-Greenstein (HG) with the same mean cosine.

where expansion coefficients are defined as

$$A_k = 2\pi(2k+1) \int_{-1}^1 p(\mu) P_k(\mu) d\mu, \quad (3)$$

we find the first few expansion coefficients

$$A_0 = 1, \quad A_1 = -\frac{4}{3}, \quad A_2 = \frac{5}{16}, \quad A_3 = 0, \quad A_4 = \frac{1}{64}, \quad A_5 = 0. \quad (4)$$

Observing that the majority of the phase function is represented by the first three terms in the expansion (Figure 2), we approximate the phase function using only these first three terms, yielding

$$p(\mu) \approx \frac{1}{4\pi} \left( \frac{27}{32} - \frac{4\mu}{3} + \frac{15\mu^2}{32} \right). \quad (5)$$

This permits us to apply an exact derivation for half space BRDFs [HC61], which we use to derive a practical fully-analytic approximation.

## 2.1. Importance Sampling

For ground-truth validation of our approximate model, we use Monte Carlo simulation of particle transport in a homogeneous half space with the LS phase function. To the best of our knowledge, there is no published procedure for importance-sampling this phase function, and we propose two such procedures here. For an exact result, we note (by considering a uniform disk projection onto a sphere together with Lambertian BRDF sampling and some simplifications) that deflection cosines can be randomly sampled with

$$\mu(\xi_1, \xi_2, \xi_3) = \sqrt{(1-\xi_1)(1-\xi_2)} \sin(2\pi\xi_3) - \sqrt{\xi_1\xi_2} \quad (6)$$

where  $\xi_1, \xi_2, \xi_3$  are three independent random numbers drawn uniformly from  $[0, 1)$ . Alternatively, with a single uniform random real  $\xi$ ,  $\mu$  can be sampled using an approximate inverse CDF,

$$\mu(\xi) \approx 1 - 2 \left( 1 - \xi^{0.0401885\xi + 1.01938} \right)^{0.397225}, \quad (7)$$

which has a maximum absolute error of  $|\mu - \mu_{exact}| < 0.0005$ . The latter procedure is likely more efficient and we recommend this sampling for use with low-discrepancy random sequences.

## 2.2. Fourier Integrals

To use a phase function in a Fourier framework such as adding/doubling [vdH80, JdJM14], we require the Fourier integrals:

$$p_l(\mu_i, \mu_o) = \frac{2 - \delta_{0l}}{\pi} \int_0^\pi p(\mu_i, \mu_o, \phi) \cos(l\phi) d\phi. \quad (8)$$

Using a three-term Legendre approximation for the Lambertian-sphere phase function (Equation 5 replacing  $p$  in Equation 8) and evaluating the phase function  $p(\mu)$  using the cosine

$$\mu = \mu_i \mu_o + \sqrt{1 - \mu_i^2} \sqrt{1 - \mu_o^2} \cos(\phi) \quad (9)$$

we find

$$p_0(\mu_i, \mu_o) = \frac{45\mu_i^2(3\mu_o^2 - 1) - 256\mu_i\mu_o - 45\mu_o^2 + 207}{768\pi}, \quad (10)$$

$$p_1(\mu_i, \mu_o) = \frac{(45\mu_i\mu_o - 64)\sqrt{(\mu_i^2 - 1)(\mu_o^2 - 1)}}{192\pi}, \quad (11)$$

$$p_2(\mu_i, \mu_o) = \frac{15(\mu_i^2 - 1)(\mu_o^2 - 1)}{256\pi}, \quad (12)$$

$$(13)$$

with  $p_k = 0$  for  $k > 2$ .

## 3. BRDF derivation

Horak and Chandrasekhar [HC61] derive the exact BRDF of a half space with a general three-term phase function,

$$c P(\cos \theta) = \omega_0 + \omega_1 P_1(\cos \theta) + \omega_2 P_2(\cos \theta) \quad (14)$$

where  $P_1$  and  $P_2$  are Legendre polynomials. Their result generalizes the special case for the non-absorbing half space, given earlier [Cha60, p.158] (see also page 6 of [Aue61] for more on the non-absorbing case, [Smo76] for a four-term phase function and [CLCC63, Sob68, VdH70] for more on the general problem). In their notation, the *single-scattering albedo*  $c$  (which here is the diffuse albedo of the spherical particles) is folded into the phase function and so, in the case of the three-term truncation given by the coefficients in Equation 4, we have

$$\omega_0 = c, \quad \omega_1 = \frac{-4c}{3}, \quad \omega_2 = \frac{5c}{16}. \quad (15)$$

The BRDF of a three-term half space is given exactly as a sum of three Fourier modes

$$f_r(\vec{\omega}_i, \vec{\omega}_o) = f^{(0)}(\mu_i, \mu_o) + f^{(1)}(\mu_i, \mu_o) \cos(\phi) + f^{(2)}(\mu_i, \mu_o) \cos(2\phi). \quad (16)$$

The functions  $f^{(i)}(\mu_i, \mu_o)$  are cone-to-cone transfer functions and are closely related to transfer matrices used in adding/doubling and related numerical methods [vdH80, JdJM14]. For light arriving from a direction with cosine  $\mu_i$ , the average radiance leaving the material along the cone with cosine  $\mu_o$  is  $f^{(0)}(\mu_i, \mu_o)$ , and the higher order terms give the discrete cosine series that determine the variation of the outgoing radiance within that cone, parametrized by relative azimuth  $\phi$ .

The functions  $f^{(i)}(\mu_i, \mu_o)$  include all orders of scattering and

are complex expressions in the case of a three-term phase function. We would like to take advantage of the known simple analytic expression for the single-scattering component of the BRDF [Cha60, HK93]

$$f_1(\vec{\omega}_i, \vec{\omega}_o) = c \frac{P(-\vec{\omega}_i \cdot \vec{\omega}_o)}{\mu_i + \mu_o}. \quad (17)$$

To exploit this result, and to further ensure that single-scattering is represented exactly, we will represent our final BRDF as the sum of single-scattering and multiple-scattering terms

$$f_r(\vec{\omega}_i, \vec{\omega}_o) = f_1(\vec{\omega}_i, \vec{\omega}_o) + f_m(\vec{\omega}_i, \vec{\omega}_o) \quad (18)$$

where the single-scattering portion is computed using Equation 17. We will therefore use the three-term expansion of the phase function only for solving for the multiple-scattering components

$$f_m(\vec{\omega}_i, \vec{\omega}_o) = f_m^{(0)}(\mu_i, \mu_o) + f_m^{(1)}(\mu_i, \mu_o) \cos(\phi) + f_m^{(2)}(\mu_i, \mu_o) \cos(2\phi).$$

These functions can be determined from the general derivation [HC61] once the corresponding  $H$  functions and constants are solved for.

### 3.1. The $H$ functions

Horak and Chandrasekhar [HC61] use invariance principles to derive the BRDF for a half space with a three-term phase function. Their derivation leads to three *pseudo problems* [Cha60, p.351] with three corresponding  $H$  functions. As these concepts are new to computer graphics, we briefly give some context here. For plane-parallel transport in a homogeneous half space with isotropic scattering, the integral equation of transport is a Fredholm integral equation of the second kind

$$C(x) = C_0(x) + c \int_0^\infty C(x') K_C(x - x') dx' \quad (19)$$

for the collision density  $C(x)$ . Solution of this equation (in particular, the Laplace transform of the solution) is related to what Chandrasekhar calls the  $H$  function, the solution of a related nonlinear integral equation

$$\frac{1}{H(\mu)} = 1 - \mu \int_0^1 \frac{H(x) \Psi(x)}{\mu + x} dx. \quad (20)$$

Once the  $H$  function is found, the BRDF for the half space is completely determined and follows rather simply [Cha60]

$$f_r(\mu_i, \mu_o) = \frac{c}{4\pi} \frac{H(\mu_i) H(\mu_o)}{\mu_i + \mu_o}. \quad (21)$$

However, once the scattering becomes anisotropic, the BRDF involves more than one  $H$  function. Each of these  $H$  functions (one for each non-zero order in the Legendre expansion of the phase function) satisfies Equation 20, but with different *characteristic*  $\Psi(\mu)$ . While each of these  $H$  functions resembles the original isotropic transport problem, on their own they do not correspond to any physical problem and so Chandrasekhar called them *pseudo problems*. In the following, we will apply known results about the solution of pseudo problems and refer the reader to related work for more details. We highly recommend Ivanov's excellent summary as a starting point [Iva94].

The characteristic functions  $\Psi^{(i)}(\mu)$  for our three-term half space

BRDF follow from inserting Equation 15 into the general solution [HC61, p.55], and we find

$$\begin{aligned}\Psi^{(0)}(\mu) &= \frac{1}{384}c \left( -15(c-1)(4c+9)\mu^4 + (c(20c+281) - 346)\mu^2 + 207 \right), \\ \Psi^{(1)}(\mu) &= -\frac{1}{192}c \left( \mu^2 - 1 \right) \left( 5(4c+9)\mu^2 - 64 \right), \\ \Psi^{(2)}(\mu) &= \frac{15}{256}c \left( \mu^2 - 1 \right)^2.\end{aligned}$$

We can then numerically evaluate the  $H$  functions using the

Fok/Chandrasekhar equation [Foc44, Kre62]

$$H^{(i)}(\mu) = \exp \left( -\frac{\mu}{\pi} \int_0^\infty \frac{1}{1+\mu^2 t^2} \log K^{(i)}(t) dt \right), \quad (22)$$

where the functions  $K^{(i)}(t)$  are given by [Kre62]

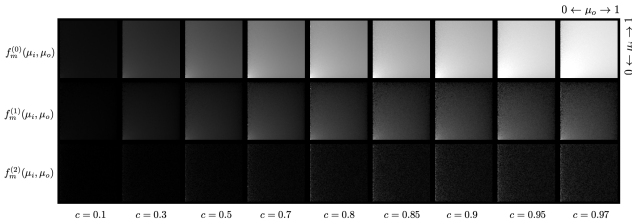
$$K^{(i)}(t) = 1 - \int_1^\infty \left( \frac{1}{s-it} + \frac{1}{s+it} \right) \frac{\Psi^{(i)}\left(\frac{1}{s}\right)}{s} ds. \quad (23)$$

Working these out, we find

$$K^{(0)}(t) = 1 - \frac{c \left( (256c - 301)t^3 + ((346 - c(20c + 281))t^2 - 15(c-1)(4c+9) + 207t^4) \tan^{-1}(t) + 15(c-1)(4c+9)t \right)}{192t^5}, \quad (24)$$

$$K^{(1)}(t) = 1 - \frac{c \left( (40c + 282)t^3 - 3(t^2 + 1)(20c + 64t^2 + 45) \tan^{-1}(t) + 15(4c+9)t \right)}{288t^5}, \quad (25)$$

$$K^{(2)}(t) = 1 - \frac{5c \left( 3(t^2 + 1)^2 \tan^{-1}(t) - t(5t^2 + 3) \right)}{128t^5}. \quad (26)$$



**Figure 3:** Using Monte Carlo reference, we observe comparatively weak signal in the second-order mode of the multiple-scattering portion of the BRDF,  $f_m^{(2)}(\mu_i, \mu_o)$  (bottom row).

We will use these with Equation 22 to numerically evaluate the  $H$  functions and form more efficient analytic approximations suitable to direct use in rendering. Alternatively, the  $H$  functions can also be evaluated using quadrature methods [Cha60, HC61].

### 3.2. Second-order Fourier mode

For the second-order Fourier mode  $f_m^{(2)}(\mu_i, \mu_o)$  of the full BRDF (Equation 16), we observe (Figure 3), using MC reference, that the multiple-scattering component  $f_m^{(2)}(\mu_i, \mu_o)$  is very weak when compared to the total energy (and even just the multiply-scattered energy) in the BRDF. This happens because the already low-frequency phase function is convolved into a nearly linear-cosine shape after two or more collisions. We exploit this properly to simplify our analytic BRDF by simply setting  $f_m^{(2)}(\mu_i, \mu_o) \approx 0$ . Thus, in our approximation all azimuthal variation of the order  $\cos(2\phi)$  is implicitly contained in the single-scattering term (Equation 17).

### 3.3. First-order Fourier mode

In Figure 3 we see that the first-order Fourier mode  $f_m^{(1)}$  of the multiple scattering is non-negligible. This requires that  $f_m$  has a term of the form  $f(\mu_i, \mu_o) \cos(\phi)$  for some function  $f$ . We approximate this term from the exact solution and this one of the key differences of our BRDF to previous approximations, which assume  $f_m^{(1)} = 0$  [Hap81, Hap02].

The exact first-order mode of the BRDF is [HC61, Eq.(43)]

$$\begin{aligned}f^{(1)}(\mu_i, \mu_o) &= \frac{cH^{(1)}(\mu_i)H^{(1)}(\mu_o)}{6\pi(\mu_i + \mu_o)} \sqrt{(1-\mu_i^2)(1-\mu_o^2)} \times \\ &\times \left( 1 + \left( l^2 + \frac{45m}{64} \right) \mu_i \mu_o + l(\mu_i + \mu_o) \right), \quad (27)\end{aligned}$$

requiring determination of two constants  $\{l, m\}$ , and the  $H$  function. We used Equation 22 and Equation 25 to fit an approximation for  $H^{(1)}(\mu)$ . We found that the separable approximation

$$H^{(1)}(\mu) \approx H^{(1)}(1)H_{c=1}^{(1)}(\mu) \quad (28)$$

with

$$H_{c=1}^{(1)}(\mu) \approx e^{-0.0894878\mu^{-1.12831\mu^3+1.85728\mu^2-1.07879\mu+0.459442}} \quad (29)$$

and

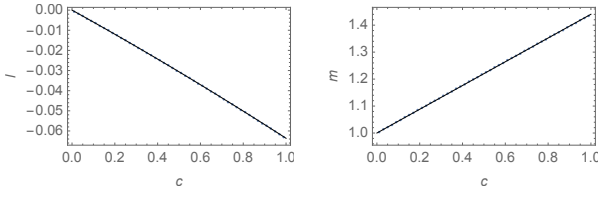
$$H^{(1)}(1) \approx e^{0.0242851c^2-0.144839c} \quad (30)$$

was accurate to within 0.5% (relative error).

Two constants  $\{l, m\}$  appear in the first-order mode, and these follow from moments of the  $H$  function [HC61, p. 56]. Using numerical evaluation of the  $H$  function moments we found the following approximations to be very accurate (Figure 4),

$$l \approx -0.00473696c^2 - 0.0589037c, \quad (31)$$

$$m \approx 0.44038c + 1. \quad (32)$$



**Figure 4:** The constants  $l$  and  $m$  appearing in the first-order mode of our BRDF are well approximated by simple approximations (continuous).

Equation 27 contains all orders of scattering. In order to use the single-scattering result exactly, we need to subtract out the approximate single-scattering from  $f^{(1)}(\mu_i, \mu_o)$  using the three-term phase function approximation. Since vectors point away from the surface in BRDF notation, we evaluate the single-scattering component using the approximate phase function evaluated with the negative cosine (Equation 9),

$$f_1^{(1)}(\mu_i, \mu_o) = \frac{1}{\pi} \int_{-\pi}^{\pi} \frac{c}{\mu_i + \mu_o} p(-\mu) \cos \phi d\phi \quad (33)$$

$$= \frac{c(45\mu_i\mu_o + 64) \sqrt{(\mu_i^2 - 1)(\mu_o^2 - 1)}}{384\pi(\mu_i + \mu_o)} \quad (34)$$

and the final multiple scattering term is

$$f_m^{(1)}(\mu_i, \mu_o) = f^{(1)}(\mu_i, \mu_o) - f_1^{(1)}(\mu_i, \mu_o). \quad (35)$$

### 3.4. Zeroth-order Fourier mode

For the zeroth-order mode we use the exact solution [HC61, Eq.(57)] to write  $f^{(0)}(\mu_i, \mu_o)$  as

$$f^{(0)}(\mu_i, \mu_o) = \frac{1}{2\pi} \frac{H^{(0)}(\mu_i)H^{(0)}(\mu_o)}{\mu_i + \mu_o} \times \left( A + B(\mu_i + \mu_o) + C\mu_i\mu_o + D\mu_i\mu_o(\mu_i + \mu_o) + E\mu_i^2\mu_o^2 + F(\mu_i^2 + \mu_o^2) \right). \quad (36)$$

Evaluation of  $f^{(0)}(\mu_i, \mu_o)$  requires numerically integrating  $H^{(0)}(\mu)$  using Equation 22 and Equation 24. To avoid this cost, we derived an approximate form inspired by the simple form that arises from the two-stream approximation with isotropic scattering [Hap81],

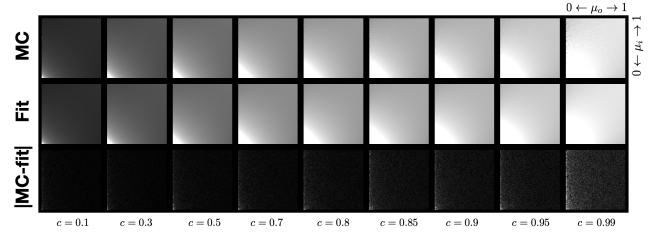
$$H^{(0)}(\mu) \approx \frac{1 + a\mu^d}{1 + \frac{a\mu^d}{H^{(0)}(\infty)}}, \quad (37)$$

where the value at infinity is [Iva94]

$$H^{(0)}(\infty) = \frac{1}{\sqrt{K^{(0)}(0)}} = \frac{12}{\sqrt{(c-16)(c-1)(4c+9)}}.$$

We used numerical-fitting methods to solve for constants  $a$  and  $d$ ,

$$a = \frac{1.50112s^{6.05435} + 8.21644}{4.17593 - 1.21222s}, \quad d = \frac{7.7731 - 0.565811s^{0.961546}}{8.65912 - 0.159974s^7},$$



**Figure 5:** Error analysis of our approximate fit for the zeroth-order transfer matrix  $f^{(0)}(\mu_i, \mu_o)$  versus a Monte Carlo (MC) reference simulation.

where  $s = \sqrt{1-c}$ . We found this to have a relative error of less than 1% in the range  $\{\mu, c\} \in [0, 1]$ .

To evaluate Equation 36 we require the constants  $A, B, C, D, E, F$ . Two of these follow from simple relations [HC61, Eq.(63)]

$$A = \frac{69c}{128}, \quad E = \frac{15}{128}(1-c)c \left( \frac{4c}{3} + 3 \right). \quad (38)$$

The other four constants involve the moments of the  $H$  function and are involved equations so we fit the following approximations

$$B = \frac{0.346689(1-c)^{3/2} - 0.777574(1-c) + 0.515357\sqrt{1-c} - 0.084463}{0.182602(1-c) - 0.665502\sqrt{1-c} + 0.964893} \quad (39)$$

$$C = \frac{-5602.45(1-c)^{3/2} + 7487.99(1-c) - 2567.74\sqrt{1-c} + 682.848}{1480.25(1-c) - 4008.33\sqrt{1-c} + 5850.6} \quad (40)$$

$$D = \frac{166.883(1-c)^{3/2} - 327.428(1-c) + 160.397\sqrt{1-c} + 0.285529}{596.423(1-c) - 412.984\sqrt{1-c} + 674.191} \quad (41)$$

$$F = \frac{266.063(1-c)^{3/2} - 21.9141(1-c) - 242.16\sqrt{1-c} - 1.9209}{215.773(1-c) + 457.42\sqrt{1-c} + 1499.9}. \quad (42)$$

The accuracy of these approximations is shown in Figure 6. We note that the last term of the last equation (for  $t$ ) on page 55 of [HC61] should read  $[\xi a_1^{(0)} - a_3^{(0)}]F$ , correcting the minus sign.

Equation 36 contains all orders of scattering. In order to use the single-scattering result exactly, we need to subtract out the approximate single-scattering from  $f^{(0)}(\mu_i, \mu_o)$  using the three-term phase function approximation. Similar to the first-order case, we compute

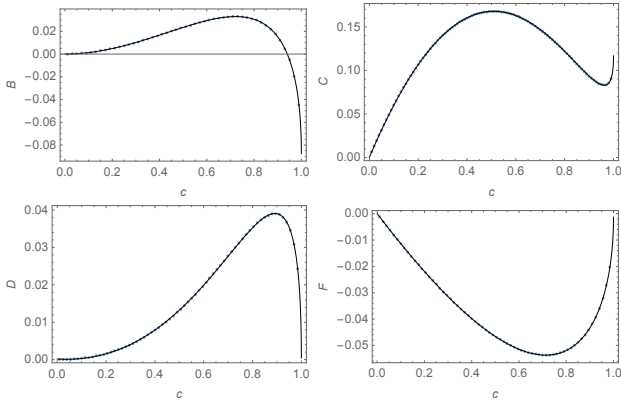
$$f_1^{(0)}(\mu_i, \mu_o) = \frac{1}{2\pi} \int_{-\pi}^{\pi} \frac{c}{\mu_i + \mu_o} p(-\mu) d\phi \quad (43)$$

$$= \frac{c \left( 207 + 135\mu_i^2\mu_o^2 - 45(\mu_i^2 + \mu_o^2) + 256\mu_i\mu_o \right)}{768\pi(\mu_i + \mu_o)} \quad (44)$$

and the final multiple scattering term is

$$f_m^{(0)}(\mu_i, \mu_o) = f^{(0)}(\mu_i, \mu_o) - f_1^{(0)}(\mu_i, \mu_o). \quad (45)$$

This completes the derivation of our approximate BRDF for the LS half space. Our analytic approximation was derived from a reciprocal and energy-conserving exact result. By construction (and



**Figure 6:** Four fitted constants (Eqs.(39) to (42)) in the zeroth-order expansion of the BRDF as a function of single-scattering albedo  $c$ . Approximation (thin) vs Exact (dots).

easily verified by inspection) our BRDF is reciprocal. For the non-absorbing case ( $c = 1$ ) our approximation loses a small ( $< 1\%$ ) amount of energy at grazing angles.

### 3.5. Albedo Mapping

We use the following fitted approximations for mapping between single-scattering albedo  $c$  of the particles in the material and  $k_d$ , the spherical/bond albedo of the material (the *diffuse color*  $k_d$  is more intuitive for artist control),

$$c = \frac{1 - (1 - k_d)^{2.73556}}{1 - 0.184096(1 - k_d)^{2.48423}}, \quad (46)$$

$$k_d = \frac{1 - 0.453029(1 - c) - 0.544162\sqrt{1 - c}}{1.42931\sqrt{1 - c} + 1}. \quad (47)$$

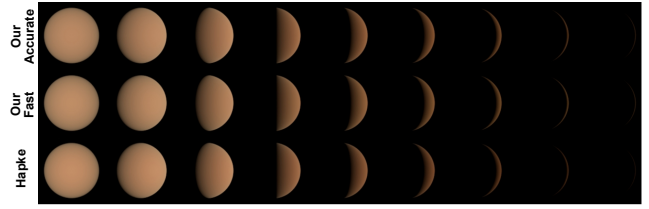
These were derived using a fitting optimization in Mathematica where the input was a table of bond albedos generated by numerically integrating our approximate BRDF.

### 3.6. Fast Variant

The analytic fitting in the previous sections still amounts to a BRDF with considerable compute cost relative to other analytic BRDFs and may be too costly for real-time applications. For more efficiency (with less accuracy) we also found the following approximation using symbolic regression software TuringBot,

$$f_r(\vec{\omega}_i, \vec{\omega}_o) = \max \left( 0, f_1(\vec{\omega}_i, \vec{\omega}_o) + 0.234459k_d^{1.85432} + \frac{0.0151829(c - 0.249978)(|\phi| + \sqrt{\mu_i\mu_o})}{\frac{\cos^{-1}(S)}{S} + 0.113706} \right), \quad (48)$$

where  $S = \sqrt{1 - \mu_i^2} \sqrt{1 - \mu_o^2}$ . Figure 7 compares the accuracy of this approximation to that of the previous section. We also compare to Hapke's approximation for general phase function [Hap81] which also includes the single-scattering component exactly but



**Figure 7:** Comparison of our accurate analytic derivation to our fast variant (Equation 48) and an approximation due to Hapke [Hap81]. Hapke's model underpredicts the reflectance at grazing angles (right). Our fast approximation offers a more accurate method with a similar computational cost to Hapke's model.

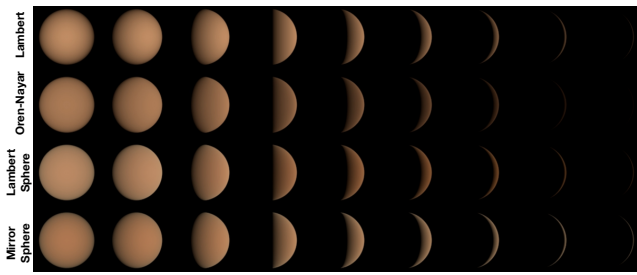
assumes and azimuthally-invariant multiple-scattering component based on the  $H$  function for the half space with isotropic scattering. All other results in the paper use the full derivation.

## 4. Results

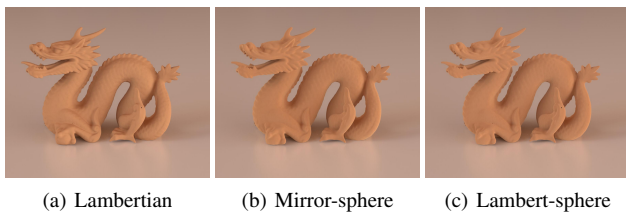
We implemented our LS BRDF in Mitsuba [Jak10], parameterized by diffuse color  $k_d$ , which is converted to a particle albedo using Equation 46. The BRDF was implemented using Equation 18 (and related equations) and uses Lambertian importance sampling. We noted a general trend of up to 30% increase in render time relative to the simpler Lambertian and Oren-Nayar [ON94] BRDFs. Some exact timings are provided in the results below. We also implemented the phase function itself for testing stochastic layer evaluations [GHZ18] and a Fourier implementation in the layer-laboratory adding/doubling framework built on Mitsuba 2 [ZJ18]. Source code will be made available.

Our LS BRDF differs significantly in appearance from standard diffusive BRDFs such as Lambertian, Oren-Nayar [ON94], and Chandrasekhar's BRDF for mirror sphere particles (Figure 8, Figure 9, Figure 10). Note the increased backscattering and saturated colors for back lighting compared to the other models. Our BRDF looks most similar to the other volumetric BRDF (Chandrasekhar's), but the bright silhouettes of Chandrasekhar's are avoided with our new BRDF (Figure 9, Figure 10).

Our volumetric BRDF can accurately model the appearance of sparse diffuse granular materials. Figure 1 shows how our model closely matches the granular microgeometry of sparse Lambertian spheres, where stochastic independent configurations of spheres increase in density to the right (300 to 1.2 million in number) while a fixed volume fraction is maintained. To compare to various sphere packings that violate the assumptions of classical radiative transfer (that the scatterers are spatially independent), in Figure 12 we consider a denser array of packings with the Lambertian albedo held fixed in all cases. We observe that height-field models can do a reasonable job at approximating such sphere cluster geometries up until about roughness  $\alpha = 2.4$ , although this requires significant stochastic evaluation to account for the many orders of scattering required to represent the full BRDF. (The Oren Nayar model only accounts for 2 bounces, and does not extend to such a range of roughnesses, appearing overly bright). Around this point the height-field assumption is inconsistent and a spherical NDF would



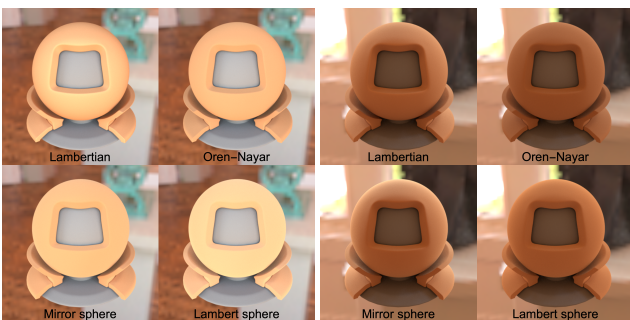
**Figure 8:** Comparison of our new BRDF to two height-field BRDFs and one volumetric BRDF (mirror-sphere) for a variety of lighting directions. Note the increased back-scattering and saturated silhouettes for back-lighting compared to the other models.



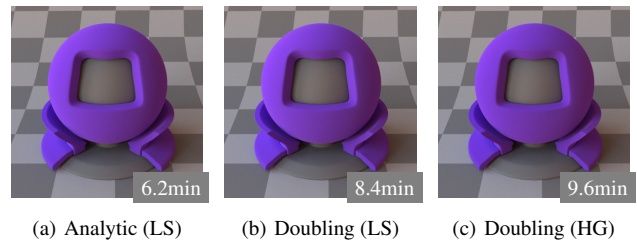
**Figure 9:** Comparison of 3 diffuse BRDFs.

be more appropriate [Dhd16]. Past this roughness level, the rough diffuse Beckmann BRDF [HD15] shows dark artifacts because the roughness simply scales a height field until the profile is unreasonably spiky [Dhd16].

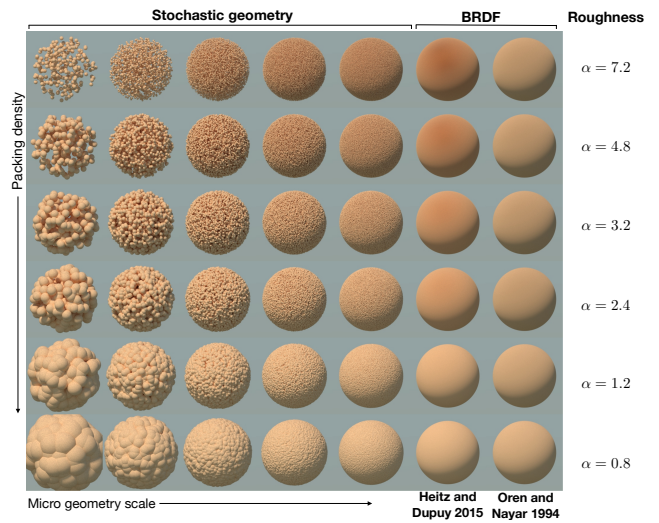
To validate our implementation we compare (Figure 11) to a result rendered using adding/doubling [JdJM14]. For a scalar RGB implementation with diffuse albedo  $k_d = (0.18, 0.05, 0.6)$ , and  $n = 60$  expansion order in  $\mu$  to avoid differences at the silhouette, the Fourier BRDF representation requires 152KiB of storage for three channels. The analytic result rendered faster with similar noise levels, despite using a simpler Lambertian importance-sampling



**Figure 10:** Comparison of our LS BRDF to three diffuse BRDFs under front lighting (left) and back lighting (right). The LS BRDF shows increased backscattering (left) and doesn't result in glowing silhouettes like Chandrasekhar's isotropic BRDF (right).



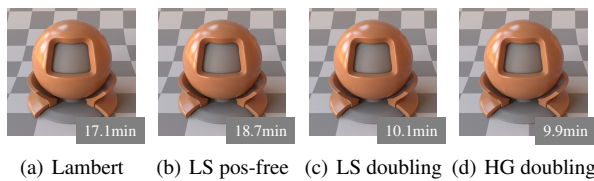
**Figure 11:** Our analytic LS BRDF (a) renders faster than the corresponding doubling method (b) and has similar noise levels despite having inferior importance-sampling. The HG BRDF with matched mean cosine has a flatter appearance under side lighting (c).  $k_d = (0.18, 0.05, 0.6)$ .



**Figure 12:** An array of granular microgeometries where the packing density and microgeometry scale vary while the diffuse albedo of the Lambertian geometry is fixed. The fine-scale appearance darkens and saturates with increased sparsity because more collisions occur (on average) before a given ray escapes the sphere and finds the light source. For dense packings (bottom rows), a random height-field is a reasonable assumption for the surface and height-field BRDFs accurately approximate the reflectance of fine-scale microgeometry (bottom right). However, for sparse granular media (top rows), the height-field assumption is inconsistent with the microgeometry, causing either dark artifacts [Heitz and Dupuy 2015] or bright unsaturated results [Oren and Nayar 1994] (top right).

scheme. The corresponding g-matched HG render is also included, showing a flatter appearance.

The assumption of sparseness challenges the physical motivation of our BRDF in isolation as there needs to be something to suspend the spheres: either a thin much sparser connective structure or a dielectric non-participating matrix suspending the Lambertian particles with an index near that of air. A more plausible scenario is the case of particles imbedded in a dielectric matrix with gen-



**Figure 13:** Rough dielectric coating ( $\alpha = 0.05$ ) over a variety of diffusive base BRDFs.

eral index  $\eta > 1$ , which we can simulate either using the doubling method or the position-free stochastic approach. We compare such dielectric coatings in Figure 13 where we layer our BRDF below a rough dielectric interface with a Beckmann roughness of  $\alpha = 0.05$ . The doubling BRDF computation produced 2 MiB of data for three channels. The position-free evaluation (b) matches the appearance of the doubling method (c) with significantly higher render time and higher noise, because the doubling method composes the entire BRDF into a single well-sampled result. However, the stochastic approach can permit non-rough coatings and requires no pre-computed data. The position-free evaluation shown uses our analytic BRDF as a surface, as opposed to evaluating the LS phase function in a volume layer (which rendered 130 times slower and presented much more noise). This illustrates a clear limitation of the position-free approach for highly-scattering, high-albedo, thick volumes and likewise shows the benefits of analytic results that encapsulate such complexity in a single result. Lambertian (a) and HG (d) bases are also shown, and the differences between them are less apparent in the coated context, but the overall trends observed in the non-coated cases remain present.

## 5. Conclusion

We have presented a new practical analytic BRDF for dusty/porous surfaces that exhibits back-scattering and saturation effects that are missing from prior models. Our derivation follows directly from an important, but nevertheless impractical, exact semi-analytic benchmark solution [HC61], beautifully summarized by van de Hulst [VdH70] as “a set of equations for which the letters in the alphabet did not suffice”. Our derivation has introduced pseudo-problem and related approximation techniques to graphics, which might inspire similar practical approximations for other low-order phase functions. The resulting BRDF offers new intuitive appearance behaviours to artists and for fitting measured data. We have also included new results for sampling the Lambertian-sphere phase function and including it in the doubling framework.

Future work includes investigation of measured data to see if this behaviour is found in real-world materials. We also want to derive a single analytic BRDF that blends from Lambertian through height-field models and into our new BRDF by considering a sequence of microgeometry like that illustrated in Figure 12 modeled using a spherical Gaussian NDF and a novel form of Smith’s model for handling such media [d’E16]. In such a formulation our new LS BRDF becomes the *infinite roughness* endpoint of a new expressive family of rough diffuse materials, which was the primary motivation for its derivation.

## 6. Acknowledgements

We thank the reviewers for helpful feedback, including a suggestion for improving the albedo mapping. We also thank M.M.R. Williams and Jakub Boksansky for reviewing an early draft, Lionel Simonot for tracking down the Lambertian-sphere phase function in Lambert’s book, and Matt Pharr for providing access to his English translation of the book.

## References

- [Aue61] AUERBACH T.: *Some applications of Chandrasekhar’s method to reactor theory*. Tech. rep., Brookhaven National Lab., Upton, NY, 1961. URL: <https://doi.org/10.2172/4792262>. 3
- [Bel18] BELCOUR L.: Efficient rendering of layered materials using an atomic decomposition with statistical operators. *ACM Transactions on Graphics (TOG)* 37, 4 (2018). URL: <https://doi.org/10.1145/3197517.3201289>. 1
- [Bli82] BLINN J. F.: Light reflection functions for simulation of clouds and dusty surfaces. In *Computer Graphics (Proceedings of ACM SIGGRAPH 1982)* (1982), vol. 16, ACM, pp. 21–29. URL: <https://doi.org/10.1145/965145.801255>. 1, 2
- [Bur12] BURLEY B.: Physically-based shading at Disney. In *ACM SIGGRAPH* (2012), vol. 2012, pp. 1–7. 2
- [Cha60] CHANDRASEKHAR S.: *Radiative Transfer*. Dover, 1960. 2, 3, 4
- [CLCC63] CHU C., LEACOCK J., CHEN J., CHURCHILL S.: Numerical solutions for multiple, anisotropic scattering. In *ICES, Electromagnetic Scattering* (1963), vol. 1, ICES, p. 567. 3
- [CT82] COOK R. L., TORRANCE K.: A reflectance model for computer graphics. In *ACM Trans. Graphic.* (1982), pp. 7–24. URL: <https://doi.org/10.1145/357290.357293>. 1
- [d’E16] D’EON E.: *The anisotropic cross-section for the spherical Gaussian medium*. Tech. rep., 2016. URL: <http://www.eugenedeon.com/wp-content/uploads/2016/07/sgcross.pdf>. 8
- [DHd16] DUPUY J., HEITZ E., D’EON E.: Additional progress towards the unification of microfacet and microflake theories. In *EGSR (EI&I)* (2016), pp. 55–63. URL: <https://doi.org/10.5555/3056507.3056519>. 1, 7
- [DJ18] DUPUY J., JAKOB W.: An adaptive parameterization for efficient material acquisition and rendering. *ACM Transactions on Graphics (TOG)* 37, 6 (2018), 1–14. URL: <https://doi.org/10.1145/3272127.3275059>. 1
- [Foc44] FOCK V.: Some integral equations of mathematical physics. *Doklady AN SSSR* 26, 4-5 (1944), 147–151. URL: <http://mi.mathnet.ru/eng/msb6183>. 4
- [GHZ18] GUO Y., HAŞAN M., ZHAO S.: Position-free Monte Carlo simulation for arbitrary layered BSDFs. *ACM Transactions on Graphics (ToG)* 37, 6 (2018), 1–14. URL: <https://doi.org/10.1145/3272127.3275053>. 1, 6
- [Hap81] HAPKE B.: Bidirectional reflectance spectroscopy: 1. theory. *Journal of Geophysical Research: Solid Earth* (1978–2012) 86, B4 (1981), 3039–3054. URL: <https://doi.org/10.1029/JB086iB04p03039>. 2, 4, 5, 6
- [Hap02] HAPKE B.: Bidirectional reflectance spectroscopy: 5. The coherent backscatter opposition effect and anisotropic scattering. *Icarus* 157, 2 (2002), 523–534. URL: <https://doi.org/10.1006/icar.2002.6853>. 2, 4
- [HC61] HORAK H. G., CHANDRASEKHAR S.: Diffuse Reflection by a Semi-Infinite Atmosphere. *Astrophys. J.* 134 (July 1961), 45. doi: 10.1086/147126. 2, 3, 4, 5, 8
- [Hd14] HEITZ E., D’EON E.: Importance sampling microfacet-based BSDFs using the distribution of visible normals. In *Computer Graphics Forum* (2014), vol. 33, Wiley Online Library, pp. 103–112. URL: <https://doi.org/10.1111/cgf.12417>. 1



- [HD15] HEITZ E., DUPUY J.: *Implementing a simple anisotropic rough diffuse material with stochastic evaluation*. Tech. rep., 2015. URL: <https://eheizresearch.wordpress.com/research/>. 1, 7
- [Hei14] HEITZ E.: Understanding the masking-shadowing function in microfacet-based BRDFs. *Journal of Computer Graphics Techniques* 3, 2 (2014), 32–91. URL: <http://jcgt.org/published/0003/02/03/>. 1
- [HHdD16] HEITZ E., HANIKA J., D'EON E., DACHSBACHER C.: Multiple-scattering microfacet BSDFs with the Smith model. *ACM Transactions on Graphics (TOG)* 35, 4 (2016), 58. URL: <https://doi.org/10.1145/2897824.2925943>. 1
- [HK93] HANRAHAN P., KRUEGER W.: Reflection from layered surfaces due to subsurface scattering. In *Proceedings of ACM SIGGRAPH 1993* (1993), pp. 164–174. URL: <https://doi.org/10.1145/166117.166139>. 3
- [Iva94] IVANOV V.: Resolvent method: exact solutions of half-space transport problems by elementary means. *Astronomy and Astrophysics* 286 (1994), 328–337. 3, 5
- [Jak10] JAKOB W.: Mitsuba renderer, 2010. <http://www.mitsuba-renderer.org>. 6
- [JdJM14] JAKOB W., D'EON E., JAKOB O., MARSCHNER S.: A comprehensive framework for rendering layered materials. *ACM Transactions on Graphics (ToG)* 33, 4 (2014), 1–14. URL: <https://doi.org/10.1145/2601097.2601139>. 1, 3, 7
- [KC17] KULLA C., CONTY A.: Revisiting physically based shading at imageworks. *ACM SIGGRAPH Course, Physically Based Shading* (2017). 2
- [KP03] KOENDERINK J., PONT S.: The secret of velvety skin. *Mach. Vision Appl.* 14, 4 (2003), 260–268. URL: <https://dx.doi.org/10.1007/s00138-002-0089-7>. 1
- [Kre62] KREIN M.: Integral equations on a half-line with kernel depending upon the difference of the arguments. *Amer. Math. Soc. Transl.*(2) 22 (1962), 163–288. 4
- [Lam60] LAMBERT J. H.: *Photometria sive de mensura et gradibus liminis colorum et umbrae*. Augustae Vindelicorum, 1760. English translation by David L. DiLaura. 2
- [MBT\*17] MENEVEAUX D., BRINGIER B., TAUZIA E., RIBARDIÈRE M., SIMONOT L.: Rendering rough opaque materials with interfaced Lambertian microfacets. *IEEE transactions on visualization and computer graphics* 24, 3 (2017), 1368–1380. URL: <https://doi.org/10.1109/TVCG.2017.2660490>. 1
- [MPBM03] MATUSIK W., PFISTER H., BRAND M., MCMILLAN L.: Efficient Isotropic BRDF Measurement. In *Proceedings of the 14th Eurographics Workshop on Rendering* (Goslar, DEU, 2003), EGRW '03, Eurographics Association, p. 241–247. URL: <https://dl.acm.org/doi/abs/10.5555/882404.882439>. 1
- [ON94] OREN M., NAYAR S. K.: Generalization of lambert's reflectance model. In *Proceedings of the 21st annual conference on Computer graphics and interactive techniques* (1994), ACM, pp. 239–246. URL: <https://doi.org/10.1145/192161.192213>. 2, 6
- [RBMS17] RIBARDIÈRE M., BRINGIER B., MENEVEAUX D., SIMONOT L.: Std: Student's t-distribution of slopes for microfacet based bsdfs. In *Computer Graphics Forum* (2017), vol. 36, Wiley Online Library, pp. 421–429. URL: <https://doi.org/10.1111/cgfm.13137>. 1
- [Smi67] SMITH B.: Geometrical shadowing of a random rough surface. *IEEE transactions on antennas and propagation* 15, 5 (1967), 668–671. URL: <https://doi.org/10.1109/TAP.1967.1138991>. 1
- [Smo76] SMOKTIY O.: Exact solution of a problem of diffuse reflection of solar radiation by a semiinfinite planetary atmosphere with a four-term scattering phase function. *Izvestiya, Atmospheric and Oceanic Physics* 12, 10 (1976), 1053–1066. 3
- [Sob68] SOBOLEV V.: Anisotropic Scattering of Light in a Semi-infinite Atmosphere. II. *Soviet Astronomy* 12 (Dec. 1968), 420. URL: <https://ui.adsabs.harvard.edu/abs/1968SvA...12..420S>. 3
- [SOPB08] SHKURATOV Y. G., OVCHARENKO A. A., PSAREV V. A., BONDARENKO S. Y.: Laboratory measurements of reflected light intensity and polarization for selected particulate surfaces. In *Light Scattering Reviews* 3. Springer, 2008, pp. 383–402. URL: [https://doi.org/10.1007/978-3-540-48546-9\\_10](https://doi.org/10.1007/978-3-540-48546-9_10). 1
- [Sta01] STAM J.: An illumination model for a skin layer bounded by rough surfaces. In *Rendering Techniques* (2001), pp. 39–52. URL: [https://doi.org/10.1007/978-3-7091-6242-2\\_4](https://doi.org/10.1007/978-3-7091-6242-2_4). 1
- [VdH70] VAN DE HULST H.: Reduction to h-functions in radiative transfer with a general anisotropic phase function. *Astronomy and Astrophysics* (1970), 9. URL: <https://ui.adsabs.harvard.edu/abs/1970A&A.....9..359V>. 3, 8
- [vdH80] VAN DE HULST H.: *Multiple light scattering*. Academic Press, 1980. 1, 2, 3
- [vGSK98] VAN GINNEKEN B., STAVRIDIS M., KOENDERINK J. J.: Diffuse and specular reflectance from rough surfaces. *Appl. Opt.* 37, 1 (1998), 130–139. URL: <http://ao.osa.org/abstract.cfm?URI=ao-37-1-130>. 1
- [Wil06] WILLIAMS M. M. R.: The albedo problem with Fresnel reflection. *Journal of Quantitative Spectroscopy and Radiative Transfer* 98, 3 (2006), 358–378. URL: <https://doi.org/10.1016/j.jqsrt.2005.05.095>. 2
- [WMLT07] WALTER B., MARSCHNER S., LI H., TORRANCE K.: Microfacet models for refraction through rough surfaces. In *Rendering Techniques (Proc. EG Symposium on Rendering)* (2007), pp. 195–206. URL: <https://dl.acm.org/doi/abs/10.5555/2383847.2383874>. 1
- [WNO98] WOLFF L. B., NAYAR S. K., OREN M.: Improved diffuse reflection models for computer vision. *International Journal of Computer Vision* 30, 1 (1998), 55–71. URL: <https://doi.org/10.1023/A:1008017513536>. 2
- [WW07] WEIDLICH A., WILKIE A.: Arbitrarily layered micro-facet surfaces. In *Proceedings of the 5th international conference on Computer graphics and interactive techniques in Australia and Southeast Asia* (2007), pp. 171–178. URL: <https://doi.org/10.1145/1321261.1321292>. 2
- [Yan97] YANOVITSKIY E. G.: *Light scattering in inhomogeneous atmospheres*. Springer, 1997. URL: <https://doi.org/10.1007/978-3-642-60465-2>. 1
- [ZJ18] ZELTNER T., JAKOB W.: The layer laboratory: a calculus for additive and subtractive composition of anisotropic surface reflectance. *ACM Transactions on Graphics (TOG)* 37, 4 (2018), 1–14. URL: <https://doi.org/10.1145/3197517.3201321>. 1, 6